Journal of Orthopaedic Translation 39 (2023) 100–112

Contents lists available at ScienceDirect

Journal of Orthopaedic Translation

journal homepage: www.journals.elsevier.com/journal-of-orthopaedic-translation

ORIGINAL ARTICLE

Exosomes from CD133$^+$ human urine-derived stem cells combined adhesive hydrogel facilitate rotator cuff healing by mediating bone marrow mesenchymal stem cells

Xiaopeng Tong [a,b,c,1], Yan Xu [a,b,c,1], Tao Zhang [a,b,c], Chao Deng [b,c], Jinrui Xun [a,b,c], Deyi Sun [a,b,c,**], Daqi Xu [a,b,c,*]

[a] Department of Sports Medicine, Xiangya Hospital, Central South University, Changsha, 410008, China
[b] Key Laboratory of Organ Injury, Aging and Regenerative Medicine of Hunan Province, Changsha, 410008, China
[c] National Clinical Research Center for Geriatric Disorders, Xiangya Hospital, Central South University, Changsha, 410008, China

ARTICLE INFO

Keywords:
CD133$^+$ urine-derived stem cell exosome
Bone marrow mesenchymal stem cell
Chondrogenic differentiation
Hydrogel
Rotator cuff healing
Bone-tendon interface

ABSTRACT

Background: The inadequate regeneration of natural tissue (mainly fibrocartilage) between tendon and bone during rotator cuff (RC) repair results in an unsatisfactory quality of RC healing. Cell-free therapy based on stem cell exosomes is a safer and more promising approach for tissue regeneration. Here, we investigated the effect of exosomes from human urine-derived stem cells (USCs) and their subpopulations (CD133$^+$USCs) on RC healing.

Methods: USCs were isolated from urine and sorted by flow cytometry to obtain CD133$^+$ urine-derived stem cells (CD133$^+$ USCs). Urine-derived stem cell exosomes (USC-Exos) and CD133$^+$ urine-derived stem cell exosomes (CD133$^+$ USC-Exos) were subsequently isolated from the cell supernatant and identified by transmission electron microscopy (TEM), particle size analysis, and Western blot. We performed in vitro functional assays to evaluate the effects of USC-Exos and CD133$^+$ USC-Exos on human bone marrow mesenchymal stem cells (BMSCs) proliferation, migration, osteogenic differentiation, and chondrogenic differentiation. In vivo experiments were performed by local injection of exosome–hydrogel complexes for the treatment of RC injury. The effects of CD133$^+$ USC-Exos and USC-Exos on RC healing were assessed from imaging, histological, and biomechanical tests.

Results: CD133$^+$ USCs were positive for CD29, CD44, CD73, CD90, CD133, but negative for CD34 and CD45. Differentiation ability test results showed that both USCs and CD133$^+$ USCs had the potential for osteogenic, chondrogenic, and adipogenic differentiation, but CD133$^+$ USCs had stronger chondrogenic differentiation ability. CD133$^+$ USC-Exos and USC-Exos could be efficiently taken up by BMSCs and promote their migration, osteogenic and chondrogenic differentiation. However, CD133$^+$ USC-Exos could promote the chondrogenic differentiation of BMSCs more than USC-Exos. Compared with USC-Exos, CD133$^+$ USC-Exos could promote the healing of bone-tendon interface (BTI) more effectively, which might be related to its ability to promote the differentiation of BMSCs into chondroblasts. Although the two exosomes exhibited the same effect in promoting subchondral bone repair in BTI, the CD133$^+$ USC-Exos group had higher histological scores and stronger biomechanical properties.

Conclusion: CD133$^+$ USC-Exos hydrogel complex may become a promising therapeutic approach for RC healing based on stem cell exosomes.

The translational potential of this article: This is the first study to assess the specific role of CD133$^+$ USC-Exos in RC healing which may be related to the activation of BMSCs by CD133$^+$ USC-Exos towards chondrogenic differentiation. Further, our study provides a reference for possible future treatment of BTI by applying CD133$^+$ USC-Exos hydrogel complex.

* Corresponding author. Department of Sports Medicine, Xiangya Hospital, Central South University, Changsha, 410008, China.
** Corresponding author. Department of Sports Medicine, Xiangya Hospital, Central South University, Changsha, 410008, China.
E-mail addresses: deyisun@csu.edu.cn (D. Sun), xudaqi96215@163.com (D. Xu).
[1] Xiaopeng Tong and Yan Xu contributed equally to this work

https://doi.org/10.1016/j.jot.2023.02.002
Received 12 October 2022; Received in revised form 5 February 2023; Accepted 10 February 2023

1. Introduction

Rotator cuff tear (RCT) is one of the most common motor system injuries, which often leads to shoulder pain and dysfunction. RC injury poses a heavy financial burden on society, with more than 4.5 million patient visits per year in the United States, which usually require surgical repair to restore the tendon-bone connection to relieve pain and restore function to the patient [1]. A previous study reported a 500% increase in RC surgery since 2001 [2]. Unfortunately, although the speed and technique of surgical repair have continued to improve, re-tear following surgical repair of RC injury remains a very common problem. Previous studies have shown that the incidence of recurrent tears after RC repair is between 20% and 40% in small to moderate RCT and as high as 94% in large tears [3–5]. The fundamental cause of the failure of RC reconstruction is the complex structure of RC insertion, slow repair, and poor regeneration ability. Histologically, RC enthesis consists of a special gradient of bone, calcified fibrocartilage, uncalcified fibrocartilage, and tendon [6]. In recent years, there has been a shift from the pursuit of improved surgical techniques to the pursuit of biological therapies to promote insertion healing. These include the use of stem cells, growth factors (GF), platelet-rich plasma (PRP), and stem cell exosome-based therapies [7].

Exosomes are secretory vesicles with physiological functions, ranging from 30 nm to 150 nm in diameter and are rich in proteins, nucleic acids, and lipids [8]. This intercellular vesicle transmission has now been proven to play an important role in many aspects of human health and disease, including development, immunity, tissue homeostasis, cancer, and neurodegenerative diseases [9]. Growing evidence has shown that exosomes are promising in regenerative medicine as effective substitutes for maternal cells due to the limitations of stem cell transplantation (e.g., immune rejection, tumorigenic risk, etc.) [8,9]. Some studies have discussed the effectiveness of BMSC exosomes and adipose mesenchymal cell (ADSC) exosomes in promoting RC injury repair [10,11]. However, the accessibility of BMSC and ADSC hinders their application for clinical use. Interestingly, urine-derived stem cells (USCs) have been identified and can be obtained from urine in a non-invasive manner [12]. USCs have clear advantages over ADSCs and BMSCs due to their simple, non-invasive isolation method and multi-lineage differentiation potential (e.g., osteogenic, chondrogenic, and adipogenic differentiation) [13–15]. In recent years, some studies have applied USCs in the repair of bone and cartilage defects and achieved good therapeutic effects [16,17]. However, the application of USC-Exos in the repair of RC injury has not been reported.

As the inherent heterogeneity of stem cell agents is increasingly recognized as influencing the effectiveness of therapeutic applications, some researchers are inclined to select specific lineage-differentiated stem cell subpopulations for the treatment of corresponding diseases [18–20]. These methods define subpopulations by identifying different antigens, typically using fluorescence-activated cell sorting (FACS) or magnetically-activated cell sorting (MACS). Chen AJ et al. identified and characterized a group of urine-derived stem cell subsets with stronger chondrogenic differentiation potential from human urine samples, and this population of cells expressed a higher proportion of CD133 [21]. We speculate that $CD133^+$ urine-derived stem subpopulation exosome might be used for BTI regenerative therapy more efficiently and effectively. Therefore, it will be interesting and meaningful to investigate whether USC-Exos and $CD133^+$ USC-Exos can accelerate RC healing.

As shown in Fig. 1A, based on previous studies on USC subpopulations, we intend to isolate $CD133^+$ USCs and extract their exosomes to explore the effects of USC-Exos and $CD133^+$ USC-Exos on BMSCs differentiation. After that, we established a rat RC injury model to evaluate the effect of $CD133^+$ USC-Exos loaded hydrogel on RC insertion healing.

2. Materials and methods

2.1. Cell isolation and subpopulation sorting

USCs were isolated from human urine according to a previously established protocol [22,23]. In short, urine was donated by 3 healthy individuals (male, 20–30 y) who signed informed consent. All procedures were approved by the Ethics Review Committee of Xiangya Hospital of Central South University. The urine was collected and placed in a 50 mL sterile centrifuge tube, centrifuged at 400×*g* for 10 min, and the supernatant was carefully removed. 10 mL PBS was added to the remaining 1 mL liquid after re-suspension, centrifuged at 200×*g* for 10 min, and the supernatant was carefully removed. Afterward, 3 mL primary culture medium was added to suspend the cells, and the cells were transferred to three wells of the 12-well plate on average. It was placed in an incubator for 48 h, and 1 mL of primary culture medium was added. After 96 h of culture, 1 mL of culture medium was taken out and 1 mL of proliferation medium was added. Thereafter, the replacement was performed every 24 h until the entire medium was replaced with proliferation fluid. Cells can be passaged when they reach 80%–90% confluence. The extracted USCs were identified as follows: CD29, CD44, CD73, CD90, CD34, and CD45. Antibodies were purchased from BioLegend (USA). USCs were sorted at P3 using the BD FACSAria™ III system (USA) to obtain $CD133^+$ subpopulation and analyzed using FlowJo 10 software (Tree Star, USA). After cell sorting, the selected cell population was amplified in the proliferation medium, which was changed every three days. P4-5 USCs and $CD133^+$ USCs were used in the following experiments. The four passage USCs and $CD133^+$ USCs were collected, and cell proliferation of the samples was assessed using Cell Counting Kit-8 (CCK-8, Osaka, Japan). The background-subtracted absorbance was measured with a microplate reader (Varioskan LUX, Thermo, USA) by measuring at 450 nm. After 7-day culture, The relative expression levels of *Runx2*, *Alp*, *Agg*, and *Sox9* genes were detected by qRT-PCR. Meanwhile, the expression of RUNX2 and SOX9 was detected by anti-RUNX2 antibody (AB76956, Abcam, USA) and anti-SOX9 (AB185230, Abcam, USA) immunofluorescence assay. The pluripotent differentiation potential (including osteogenic, chondrogenic, and adipogenic) of USCs and $CD133^+$ subpopulation of cells was assessed using osteogenic, chondrogenic, and adipogenic differentiation media (Cyagen Biosciences, Guangzhou, China) according to the manufacturer's protocol. Furthermore, immunofluorescence was used to assess osteogenic and chondrogenic differentiation.

2.2. Identification of human USC-Exos and $CD133^+$ USC-Exos

USC-Exos and $CD133^+$ USC-Exos were isolated by ultracentrifugation as described previously [22]. Briefly, USCs and $CD133^+$ USCs were obtained, washed with PBS, and cultured in USC medium without exosomes FBS (Thermo Fisher, USA). Afterward, the culture medium was collected and centrifuged at 2000×*g* for 30 min. The extracted supernatant was filtered by a 0.22-μm filter (Millipore, Billerica, USA) to remove dead cells and cell debris. Finally, the filtrate was added to an ultrafiltration tube (Millipore, USA), and centrifuged twice at 100,000×*g* for 2 h each to obtain exosome microspheres. All centrifugation procedures were performed at 4 °C. The exosome microspheres were resuspended in 200 μL PBS and stored in a −80 °C freezer for subsequent experiments. The morphology of exosomes was observed by transmission electron microscopy (TEM; Hitachi H-7650, Hitachi, Japan). The size and concentration of exosomal microspheres were determined by Nanoparticle Tracking Analysis (NTA) using the NanoSight NS3000 system (NanoSight, Amesbury, UK) as previously described [22]. Exosome protein content was determined using a BCA™ protein assay kit (Thermo Fisher, USA). The expression of exosome surface marker proteins including CD63, CD81, and TSG101 were detected by Western blot.

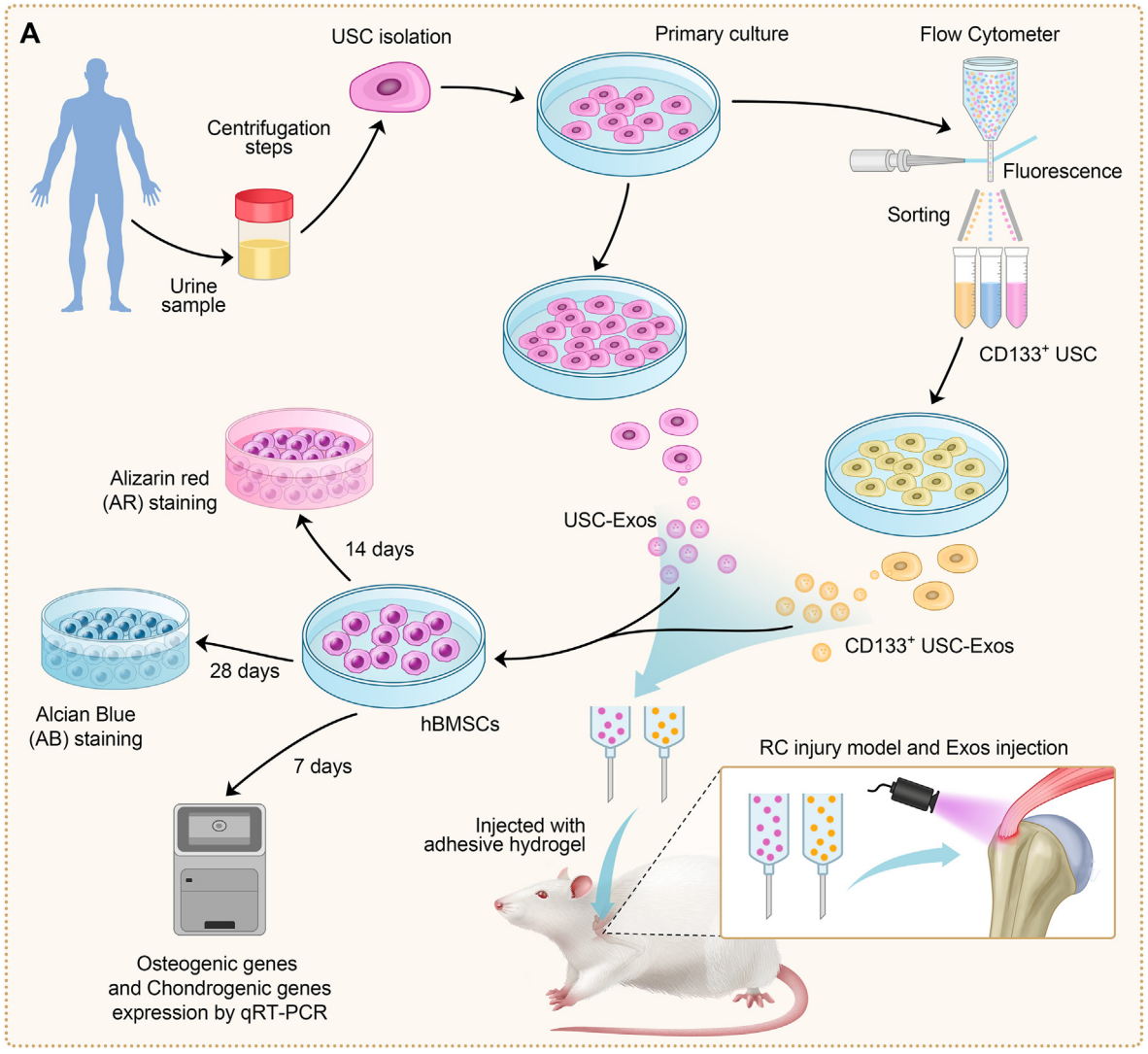

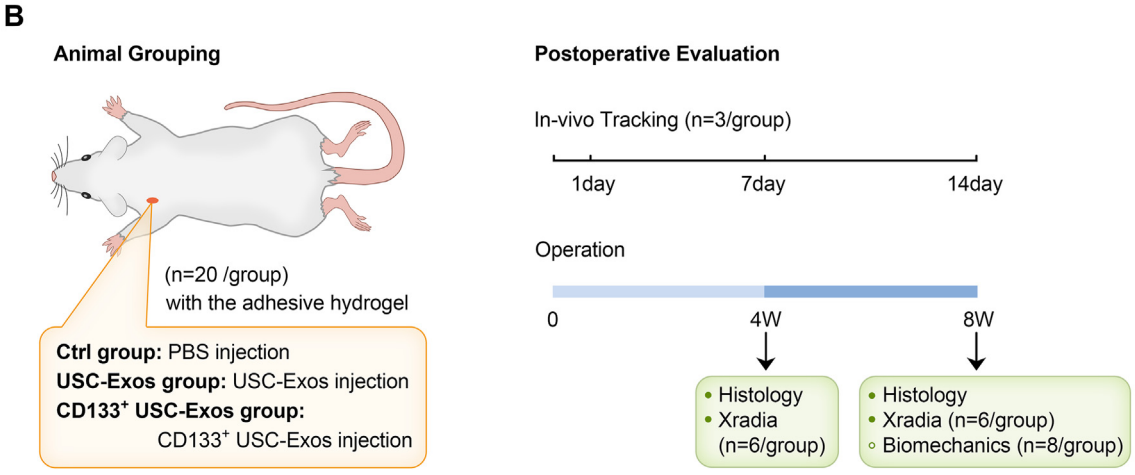

Fig. 1. Schematic diagram of the overall experimental process. (A) Schematic representation of in vitro experiments showing the effect of exosomes on the biological behavior of BMSCs and in vivo experiments showing exosomes in the treatment of rotator cuff injury in rats. (B) The experimental flow chart showing the in vivo experiments used to evaluate the effect of PBS, USC-Exos, or $CD133^{+}$ USC-Exos with the adhesive hydrogel on rotator cuff healing, in which group, point of death, number of animals in each group, and the outcome evaluation were presented.

2.3. Culture of human BMSCs

Bone marrow was donated from 4 patients aged 19–30 years with fractures (pre-operatively signed informed consent). The collected bone marrow tissue was diluted with 20 mL α-MEM medium and injected into a centrifuge tube containing 24 mL Percoll separation solution at 1800 r/min for 20 min. The middle floc layer of monocytes was carefully absorbed, and the cells were cleaned and suspended before being placed in a culture flask for culture. The cells were maintained at 37 °C with 5% CO_2 and passaged after becoming 80% confluent.

2.4. Exosomes uptake assay

USC-Exos were labeled with green fluorescent dye PKH67 (Sigma Aldrich; Saint Louis, MO, USA) and $CD133^+$ USC-Exos were labeled with red fluorescent dye PKH26 (Sigma Aldrich; Saint Louis, MO, USA) according to the manufacturer's instructions. Immediately after resuspending the exosomes in 0.5 mL of Diluent C reagent, mix with 0.5 mL of Diluent C diluted PKH67 dye or PKH26 dye. After incubation at room temperature for 4 min, 1 mL of 1% BSA was added to each reaction to stop the reaction. Subsequently, all samples were washed with PBS and centrifuged at 100,000×*g* for 2 h at 4 °C to remove excess dye. The PKH67-labeled USC-Exos and PKH26-labeled $CD133^+$ USC-Exos were respectively incubated with the cultured BMSCs for 12 h. After nuclei were stained with DAPI, exosome uptake was observed using a fluorescence microscope (BIOREVO BZ7000; Keyence; Osaka, Japan).

3. In vitro effects of USC-Exos and $CD133^+$ USC-Exos on BMSCs

3.1. Cell differentiation

To examine the effects of USC-Exos and $CD133^+$ USC-Exos on the differentiation ability of BMSCs, they were seeded on 12-well plates, incubated in α-MEM medium for 12 h, and then subjected to different conditions. BMSCs were added to osteogenic differentiation and chondrogenic differentiation (Cyagen Biosciences, Guangzhou, China) medium. Then the PBS (control), USC-Exos (treated with 100 μg/mL exosomes from USCs), and $CD133^+$ USC-Exos (treated with 100 μg/mL exosomes from $CD133^+$ USCs) were added to the differentiation medium. The medium and exosomes were changed every 2 days and cultured in a 37 °C and 5% CO_2 incubator. After 7-day culture, the relative expression levels of *Runx2*, *Alp*, *Agg*, and *Sox9* genes were detected by qRT-PCR. Meanwhile, the expression of RUNX2 and SOX9 was detected by anti-RUNX2 antibody (AB76956, Abcam, USA) and anti-SOX9 (AB185230, Abcam, USA) immunofluorescence assay. Alizarin red S staining and Alcian blue staining were performed on days 14 and 28 respectively to evaluate the osteogenic and chondrogenic abilities of BMSCs.

3.2. Proliferation assay

After BMSCs were collected and recorded, cells (5×10^3 cells per well; 3 replicates in each group) were inoculated into 96-well culture plates. Then exosomes of different groups (100 μg/mL) or an equivalent amount of PBS were added to the culture medium.

On days 1, 2, 3, 5, 7, and 9, cell proliferation was assessed using the cell counting kit −8 (CCK-8, Osaka, Japan). The background-subtracted absorbance was measured with a microplate reader (Varioskan LUX, Thermo, USA) by measuring at 450 nm.

3.3. Scratch wound healing assay

BMSCs (5×10^5 cells per well; three replicates per group) were seeded on 6-well plates and incubated overnight in an incubator. After the cells had been attached, the monolayers were scraped with a sterile P200 pipette tip and rinsed three times with PBS. The α-MEM (supplemented with 1% EV-depleted FBS) medium was added, followed by the addition of different groups of exosomes (100 μg/mL) or an equivalent amount of PBS to the medium. Images were taken at 0, 12, and 24 h. Image J (Version 1.8.0, USA) was used to analyze the migration area, and the calculation formula of wound healing rate was: (A1-A2)/A1 × 100, where A1 represented the initial wound area and A2 represented the remaining wound area at the specified time point.

3.4. Transwell migration assay

The chemotactic response of BMSCs treated with different USC-Exos was studied by the transwell system (Corning, NY, USA). Briefly, 1×10^4 cells were seeded in the upper chamber, 500 μL α-MEM (supplemented with 1% Exo-depleted FBS) was added to the lower chamber, and different groups of exosomes (100 μg/mL) or the same amount of PBS were added to the medium. After 12 h, the cells at the bottom of the filter were fixed with paraformaldehyde and stained with crystal violet for 30 min. Cells from the upper chamber filter were then carefully wiped off with a cotton swab. The number of migrated cells was quantified under light microscopy (Leica).

3.5. Quantitative real-time PCR (qRT-PCR)

Total mRNA was extracted from cells using TRIzol Reagent (Invitrogen) according to the manufacturer's instructions. cDNA was generated using 1 μg RNA with a reverse transcriptase kit (Promega, Fitchburg, Wisconsin, USA). qRT-PCR was performed on the ABI PRISM 7900HT system (Applied Biosystems, Foster City, CA, USA). Relative gene expression was calculated using the $2^{-\Delta\Delta CT}$ method and GAPDH was used as normalization. The primer sequences used for qRT-PCR were as follows: *Runx2*: forward, 5′-CACTGGCGCTGCAACAAGACCCT-3′ and reverse, 5′-CCGGC CCA-CAAATCTCAGATCGT-3′; *Alp*: forward, 5′-ACCACCACGAGAGTGAACCA-3′ and reverse, 5′-CGTTGTCTGAGTACCAGTCCC-3′; *Sox9*: forward, 5′-TACACACAGCTCACTCGACCT-3′ and reverse, 5′-TTGGTCCTCTCTT TCTTCGGTT-3′; *Agg*: forward, 5′-AACAATGCCCAAGACTACCAG-3′ and reverse, 5′-TTCCACTCGCCCTTCTCGT-3′; *GAPDH*: forward, 5′-CTGGG CTACACTGAGCACC-3′ and reverse, 5′-AAGTGGTCGTTGAGGGCAATG-3′.

3.6. Exosomes loaded on adhesive hydrogel

The preparation of adhering hydrogels and the preparation of exosomes supported by adhering hydrogels were the same as in our previous report [24]. Briefly, the hydrogel consists of a certain proportion of GelMA, HA-Nb, and a photoinitiator (LAP). The hydrogel can be transformed into a gel state by irradiating it with an ultraviolet lamp with a wavelength of 365–405 nm at 37 °C for 30 s. The preparation process of the adherent hydrogel-loaded exosomes was as follows: 10 μg/μL $CD133^+$ USC-Exos and USC-Exos suspensions were collected and then added into the hydrogel solution to form a complex with a final concentration of 1 μg/μL. Then, 100 μL of the composite was then irradiated under a UV lamp to generate $CD133^+$ USC-Exos and USC-Exos supported by the adhesive hydrogel.

3.7. Rotator cuff injury repair model and exo treatment

All animal experiments and care procedures were approved by the Animal Ethics Committee of Central South University and conformed to the guidelines for reporting in vivo experiments in animal research [25]. Male Sprague–Dawley rats (300–350 g) underwent left RC repair surgery as reported in previous studies [26]. Briefly, after rats were anesthetized with 3% pentobarbital (50 mg/kg; Sigma–Aldrich, St. Louis, MO), a longitudinal incision was made on the skin surface of the left shoulder. The deltoid was incised to expose the RC insertion. After placing a 5–0 PDS wire (No. 5–0, Ethicon, NJ, USA) into the supraspinatus tendon (SST), the SST insertion was separated at its attachment to the humerus with an 11 blade. The fibrocartilage and part of the subchondral bone at the insertion point were then cured, and a 22-gauge needle was used to

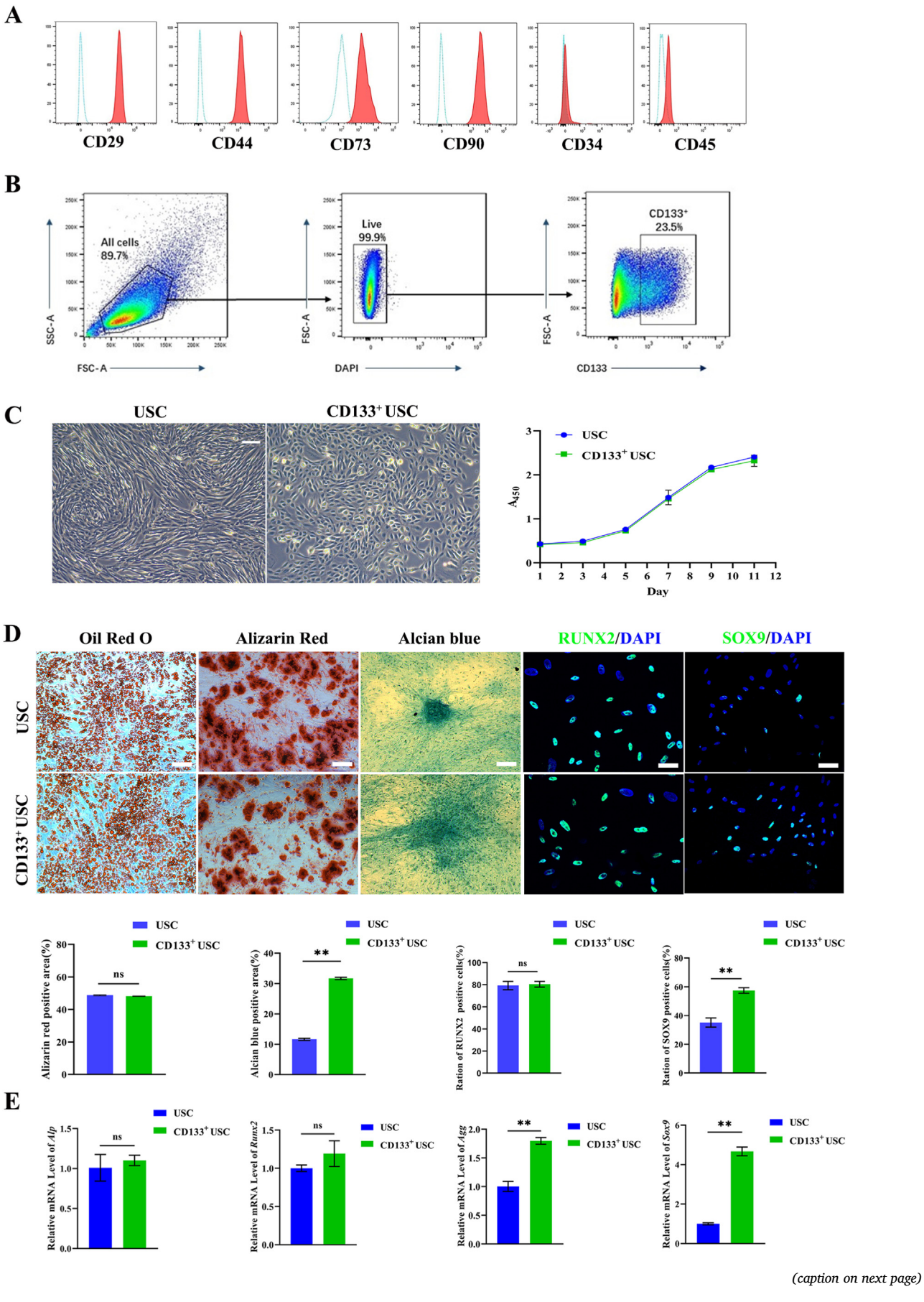

(caption on next page)

Fig. 2. CD133$^+$ USC extraction and identification of three-lineage differentiation ability. (A) Flow cytometry for the isolated cells. Representative histograms demonstrating positive and negative staining of urine-derived cells from a single human. (B) Gating strategy used to sort the CD133+ USC isolation. Representative FACS plots with the percentage of parent gate for CD133+ USC isolation. (C) Morphology of cells isolated from human urine and the CD133$^+$ USC, the proliferation of urine-derived cells was determined by CCK-8 assay. At P4, spindle-shaped or rise-shaped cells were observed. Scale bar = 50 μm. The proliferation of urine-derived cells was determined by CCK-8 assay. n = 4 for each group for each time point. (D) The ability of three lineages differentiation between USC and CD133$^+$ USC in vitro. Alizarin Red staining, Oil Red O staining, and Alcian Blue staining of the two groups. The SOX9 and RUNX2 protein expression of the two groups after 7 days of chondrogenic and osteogenic induction. Scale bar = 50 μm. n = 4 for each group. (E) Osteogenic gene (*Runx2*, *Alp*) and chondrogenic gene (*Sox9*, *Agg*) expression compared between the two groups in the osteogenic medium and chondrogenic cultures, respectively. n = 3 for each group. Data are showed as means ± standard deviation (*$P < 0.05$, **$P < 0.01$). (For interpretation of the references to color in this figure legend, the reader is referred to the Web version of this article.)

create a bone tunnel laterally through the proximal humerus. The PDS wire is passed through the bone tunnel to secure the SST to the original implantation site of the tendon. For the administration of CD133$^+$ USC-Exos and CD133$^+$ USC-Exos, after RC injury modeling, the 100 μL PBS-hydrogel complex solution, 100 μL CD133$^+$ USC-Exos (1 μg/μL), and USC-Exos (1 μg/μL) hydrogel solution were locally administered to the insertion site, cured by UV irradiation and then sutured the deltoid muscle and skin layer by layer. Postoperatively, penicillin G was used to prevent infection once a day for three days. Rats with RC injury were randomly divided into 3 groups, control group (PBS-hydrogel treatment), USC-Exos group, and CD133$^+$ USC-Exos group. The subchondral bone repair was assessed using bone morphological parameters, followed by histological and biomechanical assessment of RC healing.

3.8. In vivo imaging of DiR-labeled exo in RC injury models

To track the distribution intensity changes of Exo over time in vivo, we labeled Exo with the tracer DiR (Invitrogen, Life Technologies) as previously described [22] and embedded it in a hydrogel, which was then implanted on the RC insertion. Animals were placed in a non-invasive tracking system (Xenogen IVIS, USA) at 1, 7, and 14 days after surgery to detect the intensity and distribution of DiR in the shoulders of rats to partially detect the degradation of preloaded DiR-labeled exosomes.

4. Xradia scanning

The RC specimens were fixed in 4% paraformaldehyde for 24 h and washed with PBS. The fixed specimens were fixed on the Xradia 410 versa (Zeiss, Germany) stage. The scanning parameters were set as follows: voltage 80.0 kV, power 10 W, exposure time 1 s, and the sample-to-detector distance was 2.45 cm. 1601 ray projection images were collected by the detector, and the pixel size was 9.68 μm. Three-dimensional reconstruction and visualization of tomographic images were performed using Dragonfly (version 2021.3, ORS, Canada) software. After obtaining the 3D reconstructed image, a custom-made 3.5 mm × 3.5 mm cylindrical region of interest (ROI) at the enthesis was used to calculate the bone volume fraction (BV/TV), trabecular thickness (Tb.Th), and trabecular number (Tb.N). The researchers were blinded to both grouping and healing time.

4.1. Histological evaluation

After Xradia Scanning, samples were decalcified, dehydrated in gradients, and embedded in paraffin. The samples were sectioned to 5 μm along the sagittal plane of the supraspinatus tendon-humeral head. The tissue sections were stained with hematoxylin and eosin (H&E) to observe the morphology of BTI, and toluidine blue/fast green (TB&FG) (Sigma–Aldrich, St. Louis, MO) to observe the distribution of the fibrocartilage layer. Representative sections were scanned and imaged (Hamamatsu, NanoZoomer S360) and viewed using image viewing software (NDP.view 2.9.22 RUO). A semiquantitative analysis of BTI healing was performed by two blinded observers based on a previously reported modified bone-tendon score [27,28] (Table S1). A higher score of the SST insertion indicates a more mature BTI healing.

4.2. Biomechanical testing

The failure load and stiffness of the repair enthesis were tested using a biomechanical testing system (model 5942, Instron, MA). The total failure work can be obtained by calculating the area under the load–displacement graphs. After careful removal of sutures and excess tissue under the microscope, the SST was sanded in the upper clamp and the humeral shaft was fixed in the lower clamp. The tendon-humeral complexes were positioned to allow longitudinal stretch in the direction of the tendon attachment site. The samples were loaded to failure at a rate of 14 μm/s after a 0.1 N preload. The test was performed at room temperature and 0.9% saline was used to avoid drying of the specimens.

4.3. Statistical analysis

Statistical analyses were performed using SPSS 25.0 software (SPSS, USA). All quantitative data were expressed as mean ± standard deviation (SD). Data were confirmed normal distribution by Shapiro–Wilk test and homoscedasticity by Levene's Test before t-test analysis and One-way ANOVA analysis. Unpaired two-tailed Student's t-test was used to determine statistical significance between two groups, while the histological scores were performed using the Mann–Whitney test. One-way ANOVA with post hoc test was used to analyze the differences above two groups. $P < 0.05$ was considered statistically significant.

5. Results

5.1. Identification of CD133$^+$ USCs and CD133$^+$ USC-Exos

USCs were successfully isolated from human urine, and flow cytometry analysis showed that USCs were highly positive for the surface markers CD29, CD44, CD73, and CD90, but negative for CD34 and CD45 (Fig. 2A). The CD133$^+$ USCs obtained by subsequent sorting by flow cytometry were positive for the surface marker CD133 (Fig. 2B). Most of the USCs exhibited a spindle-shape, while CD133$^+$ USCs appeared a rise-shape (Fig. 2C). The results of CCK-8 analysis showed that no significant difference was observed in the proliferative capacity between USCs and CD133$^+$ USCs (Fig. 2C). To assess whether USCs and CD133$^+$ USCs cells have tri-lineage differentiation potential, positive results of alizarine red S staining, oil red O stainingand Alcian blue staining showed that USCs and CD133$^+$ USCs could achieve targeted differentiation in osteogenic, chondrogenic and lipogenic differentiation media (Fig. 2D). Quantification of the degree of differentiation showed that the CD133$^+$ USCs showed higher chondrogenic differentiation, but they were no significant differences in osteogenic and adipogenic differentiation abilities (Fig. 2D). Immunofluorescence analysis also showed that the proportion of SOX9 positive cells in CD133$^+$ USC Exos group was significantly higher than that in USC group, but there was no difference in the proportion of RUNX2 positive cells between the two groups (Fig. 2D). When compared with the USCs, the CD133$^+$ USCs showed significantly higher expressions of *Sox9* and *Agg* at 7 days (Fig. 2E). These data indicated that CD133$^+$ USCs had stronger chondrogenic expression and chondrogenic differentiation ability compared with USCs. Transmission electron microscopy revealed the spherical morphology of USC-Exos and CD133$^+$ USC-Exos (Fig. 3A). The diameter distribution of exosomes ranged from 50 to 150 nm (Fig. 3A). Western blot results showed that both USC-Exos

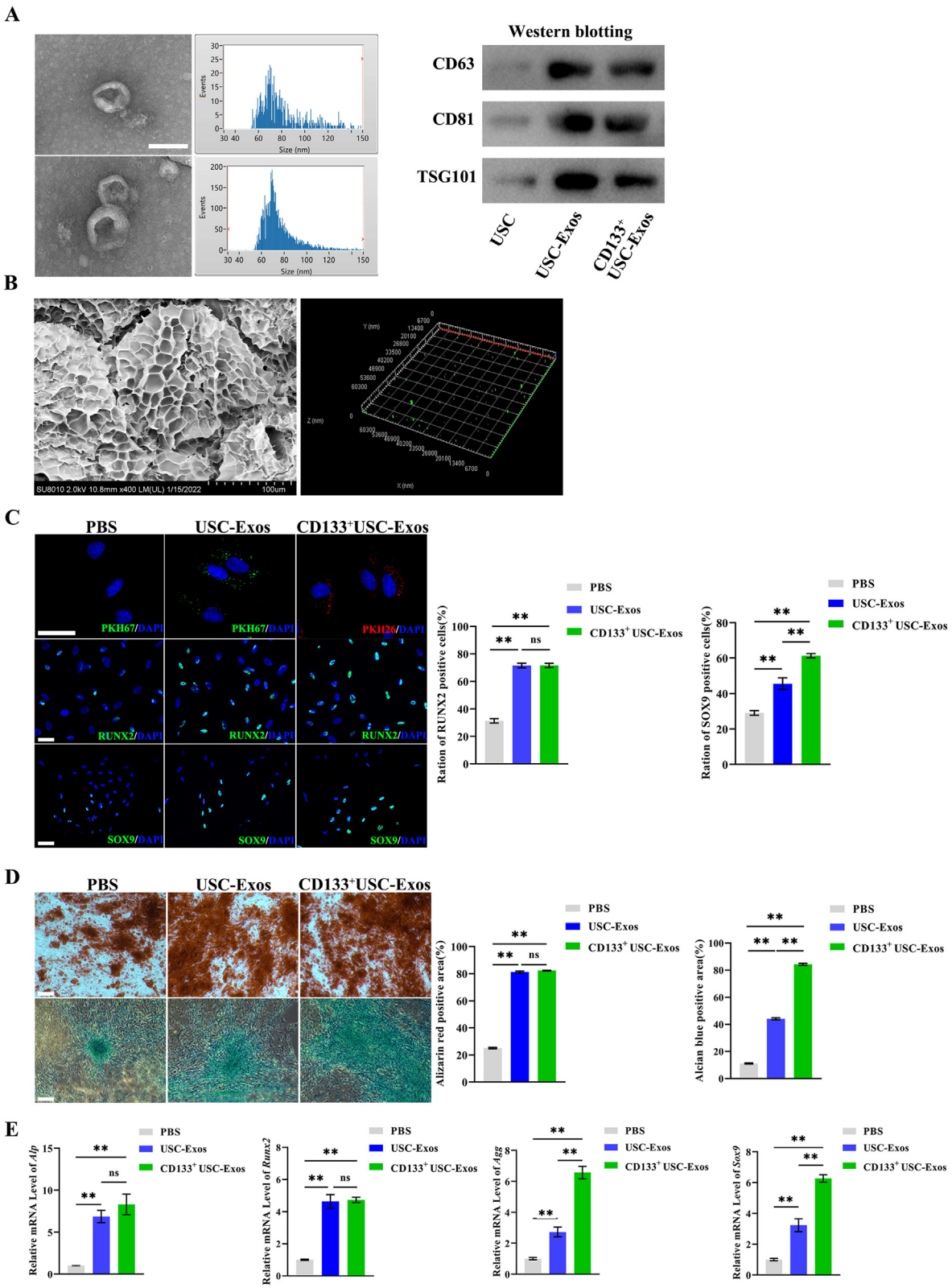

Fig. 3. CD133$^+$ USC-Exos can better promote the chondrogenic differentiation of BMSCs than USC-Exos. (A) Identification and characterization of USC-Exos and CD133$^+$ USC-Exos by observing their morphology, measuring particle size distribution, and evaluating the expression of exosomal markers. Scale bar = 100 nm. (B) Electron microscopy and confocal microscopy of hydrogels containing exosomes. The exosomes are labeled with PKH26 dye. (C) Uptake of the exosomes, CD133$^+$ USC-Exos significantly promoted the SOX9 expression of BMSCs. Uptake of the green fluorescence dye PKH67-labelled USC-Exos and the red fluorescence dye PKH26-labelled CD133$^+$ USC- Exos into BMSCs. Scale bar = 50 μm. (D) Alizarin Red staining and Alcian Blue staining of BMSCs after culturing with USC-Exos and CD133$^+$ USC-Exos. Comparative analysis of Alizarin Red staining and Alcian Blue staining area after BMSCs cultured with PBS, USC-Exos, and CD133$^+$ USC-Exos. (E) The relative expression levels of *Runx2*, *Alp*, *Agg*, and *Sox9* genes of BMSCs under different conditions. Bar = 50 μm. n = 3 for each group. Data are showed as means ± standard deviation (*$P < 0.05$, **$P < 0.01$). (For interpretation of the references to color in this figure legend, the reader is referred to the Web version of this article.)

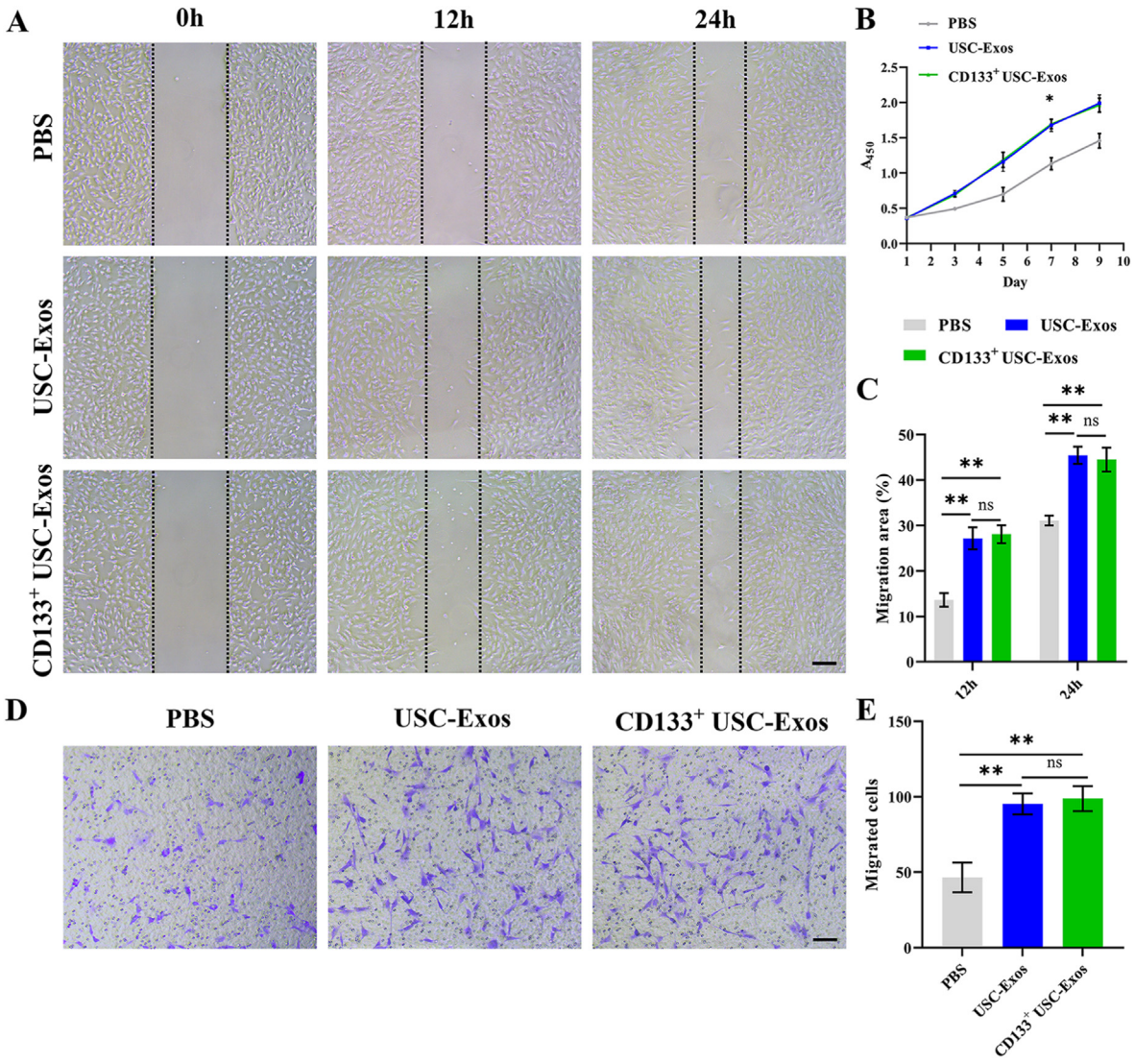

Fig. 4. USC-Exos and CD133$^+$ USC-Exos enhance the proliferation and migration of BMSCs. (A) Representative images of scratch wound assay in BMSCs treated with PBS, USC-Exos or CD133$^+$ USC-Exos. Scale bar = 200 μm. (B) The proliferation of BMSCs receiving different treatments was tested by CCK-8 analysis. n = 3 per group. (C) Quantitative analysis of the migration rates in (A). n = 4 per group. (D) The migration of BMSCs stimulated by USC-Exos, CD133$^+$ USC-Exos or an equal volume of PBS was detected by the transwell assay. Scale bar = 100 μm. (E) Quantitative analysis of the migrated cells in (D). n = 4 per group. Data are showed as means ± standard deviation (*$P < 0.05$, **$P < 0.01$).

and CD133$^+$ USC-Exos expressed exosome markers CD63, CD81 and TSG101 (Fig. 3A). The above data indicated that the acquisition of USC-Exos and CD133$^+$ USC-Exos was successful.

Analysis of USC-Exos and CD133$^+$ USC-Exos in promoting osteogenic and chondrogenic differentiation in vitro

To determine the effect of CD133$^+$ USC-Exos and USC-Exos on the differentiation of BMSCs, we first determined whether these two Exos could be internalized into these cells. The results showed that both BMSCs successfully internalized CD133$^+$ USC-Exos and USC-Exos (Fig. 3C). Immunofluorescence assay showed that the proportion of SOX9 positive cells in CD133$^+$ USC-Exos-treated BMSCs was significantly higher than that in USC-Exos-treated BMSCs (Fig. 3C). Alizarin red S staining showed that both CD133$^+$ USC-Exos and USC-Exos significantly enhanced the formation of calcium nodules in BMSCs, and the quantitative results showed that there was no statistical difference between the two in promoting osteogenesis of BMSCs (Fig. 3D). The results of alcian blue staining showed that both exosomes could significantly promote the chondrogenic differentiation of BMSCs, while the cartilage of BMSCs after subgroup exosome intervention showed higher chondrogenic differentiation (Fig. 3D). The effect of exosomes on osteogenic and chondrogenic differentiation of mesenchymal stem cells was detected by qRT-PCR at gene level. Compared with the control group, the expressions of bone-specific genes (*Runx2* and *Alp*) and hyaline cartilage-specific genes (*Sox9* and *Agg*) of BMSCs treated with Exo were significantly up-regulated (Fig. 3E). Compared with USC-Exos-treated BMSCs, *Sox9* and *Agg* levels were significantly higher in CD133$^+$ USC-Exos-treated BMSCs, while *Runx2* and *Alp* levels were not significantly different between the two groups (Fig. 3E). These data suggested that CD133$^+$ USC-Exos might influence RC healing more by activating chondrogenic differentiation of BMSCs than USC-Exos.

5.2. Analysis of CD133$^+$ USC-exos and USC-exos in promoting BMSCs proliferation and migration in vitro

CCK-8 assay showed that BMSCs exhibited a much stronger proliferative ability when exposed to USC-Exos and CD133$^+$USC-Exos, but there was no difference in the ability of these two exosomes to promote BMSCs proliferation (Fig. 4B). Scratch test results (Fig. 4A–C) and transwell assay results (Fig. 4D and E) showed that the lateral and longitudinal migration abilities of BMSCs treated with both Exos were

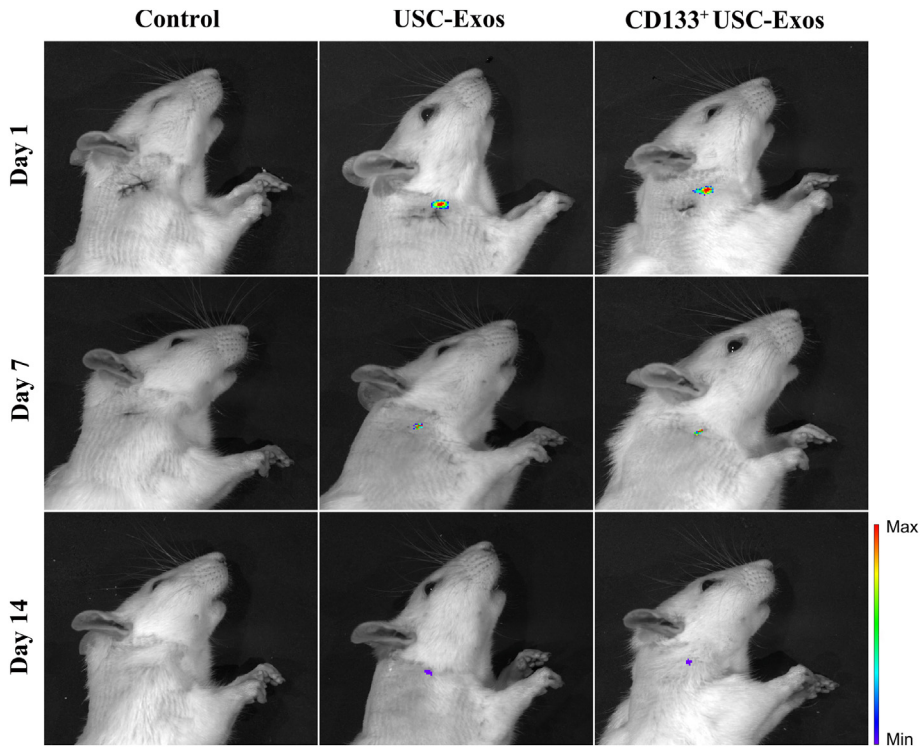

Fig. 5. The adhesive hydrogel-loaded CD133$^+$ USC-Exos and USC-Exos have sustained-release properties. In-vivo tracking of the operatine site injected PBS, DiR-labeled USC-Exos, or CD133$^+$ USC-Exos with the adhesive hydrogel. Scale bar = 5 mm.

significantly enhanced compared with those treated with PBS, while there was no statistically significant difference between CD133$^+$ USC-Exos and USC-Exos groups. The above experimental results suggested that either CD133$^+$ USC-Exos or USC-Exos could significantly promote the proliferation and recruitment of BMSCs, and there was no difference in the ability of these two types of exosomes to recruit stem cells and promote stem cells proliferation.

5.3. *The adhesive hydrogel sustained the release of USC-Exos and CD133$^+$ USC-Exos in-vivo*

The results showed that exosomes and hydrogel complexes were successfully prepared, and exosomes were evenly distributed in the hydrogel (Fig. 3B). As shown in Fig. 5, we tracked the distribution of dir-labeled exosomes embedded in hydrogels after topical treatment in vivo with the Xenogen IVIS imaging system. The red fluorescence signals were observed for at least 14 days at RC lesions, indicating that the adhesive hydrogel-loaded CD133$^+$ USC-Exos and USC-Exos had sustained-release properties.

5.4. *Xradia analysis*

Bone repair at the insertion site was assessed by 3D reconstruction images and quantitative analysis of bone morphological parameters (Fig. 6A and B). There was significant bone loss in the subchondral bone of BTI in all groups at 4 weeks postoperatively. BTI had obvious new bone formation at 8 weeks postoperatively (Fig. 6A). Quantitatively, BV/TV, Tb.Th, Tb.N in CD133$^+$ USC-Exos and USC-Exos groups were significantly improved compared with the control group at 4 and 8 weeks after surgery (Fig. 6B). However, there was no statistically significant difference in BV/TV, Tb.Th, Tb.N between CD133$^+$ USC-Exos and USC-Exos groups. These data suggested that both CD133$^+$ USC-Exos and USC-Exos could promote BTI new bone formation, but the promoting effects of the two were consistent.

5.5. *Histological analysis*

H&E and TB&FG staining results showed that the healing morphology of rat BTI was gradually improved with the extension of healing time (Fig. 7A). The BTI tissue of the rat in the USC-Exos and CD133$^+$ USC-Exos groups had good continuity, with relatively neat and orderly fibers, and a new fibrocartilage layer appeared, while the control group had poor tissue continuity, disordered fibers, and no obvious fibrocartilage layer generation at 4 weeks postoperatively. Histological scores showed that the scores of the CD133$^+$ USC-Exos group were better than those of the USC-Exos group and the control group (Fig. 7C). The score of the USC-Exos group was better than that of the control group, and there was a statistical difference between the two groups (Fig. 7C). The CD133$^+$ USC-Exos and USC-Exos groups had more mature tendon-bone attachments than the control group at 8 weeks postoperatively. Compared with the control group and the USC-Exos group, the fibrocartilage layer in the CD133$^+$ USC-Exos group was significantly thicker, and the polarity of the cells and fibers was better arranged. The histological score showed that the score of the USC-Exos group was better than that of the control group and there was a statistical difference (Fig. 7C). Interestingly, the CD133$^+$ USC-Exos group scored significantly higher than the other groups (Fig. 7C). The above results indicated that both CD133$^+$ USC-Exos and USC-Exos could promote the healing of BTI during the healing process of RC injury in rats, but the former has a more obvious effect on the repair of insertion.

5.6. *Biomechanical testing*

Biomechanical properties are important indexes to evaluate the healing quality of BTI (Fig. 8). In the biomechanical test, all specimens ruptured at the surgical repair site. The failure load, stiffness, and total work to failure of the CD133$^+$ USC-Exos group were significantly higher than those in the USC-Exos group and control group at 8 weeks after surgery (Fig. 8B). These results indicated that CD133$^+$ USC-Exos could

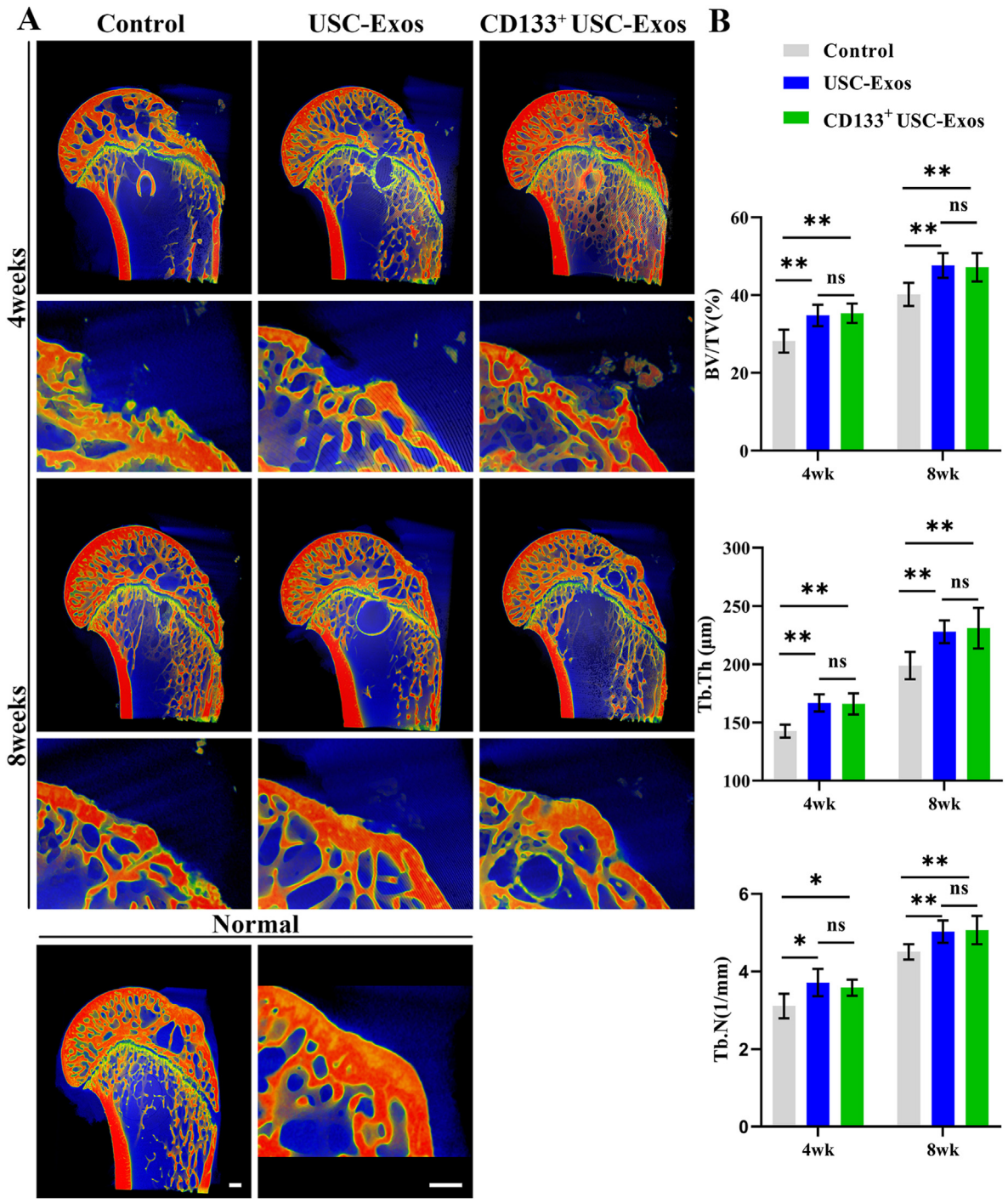

Fig. 6. USC-Exos and CD133$^+$ USC-Exos facilitate subchondral bone repair of RC insertion. (A) Representative Xradia scanning images of the RC healing site in the Control, USC-Exos, and CD133$^+$ USC-Exos groups at postoperative 4 weeks and 8 weeks. Scale bar = 100 μm. (B) Representative Xradia scanning images of RC enthesis for normal group. (C) Comparison of the bone volume/total volume (BV/TV), trabecular thickness (Tb.Th), trabecular number (Tb.N) in newly formed bone among all groups at different time points after RC injury repair. n = 6 per group. Data are showed as means ± standard deviation (*$P < 0.05$, **$P < 0.01$).

promote the recovery of RC biomechanical properties more effectively than USC-Exos.

6. Discussion

The major challenge in RC healing process is the unsatisfactory BTI healing potential due to its insufficient regeneration of the native tissue (mainly fibrocartilage) between tendon and bone. How to effectively promote tendon-bone healing is the key to treating RC injury and preventing re-tear after surgery. Cell-free therapy such as exosome treatment has advantages like non-immune rejection, non-tumorigenicity, and high stability, and is an option for the treatment of various diseases, which is a safer and more promising approach [11,29,30]. To our knowledge, this is the first time that local injection of USC-Exos and CD133$^+$ USC-Exos has been used to evaluate their functional roles in facilitating BTI regeneration in RC injury model. In this study, after the noninvasive acquisition of USCs and CD133$^+$ USCs from human urine, USC-Exos and CD133$^+$ USC-Exos were extracted and

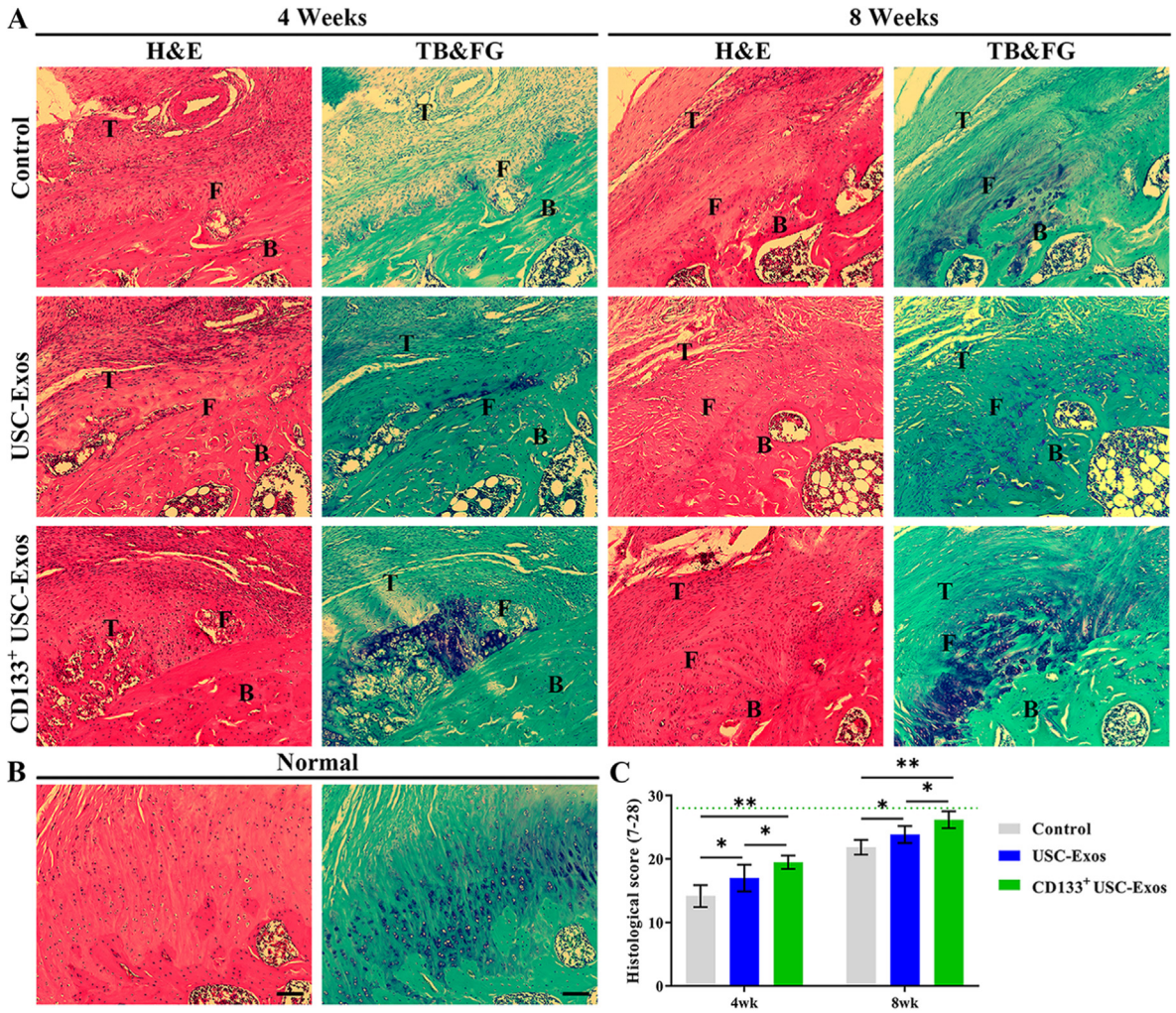

Fig. 7. CD133$^+$ USC-Exos promote the healing of bone-tendon interface (BTI). (A) Representative histologic images of RC enthesis at 4 weeks and 8 weeeks post-operatively for all groups. (B) Representative histologic images of RC enthesis for normal group. (C) Histological maturing scores for RC insertion. The green dolt line indicated the perfect histological score of 28. n = 6 per group. T: tendon; F: fibrocartilage; B: bone, H&E: hematoxylin and eosin; TB&FG: toluidine blue and fast green. Scale bar = 500 μm. Data are showed as means ± standard deviation (*$P < 0.05$, **$P < 0.01$). (For interpretation of the references to color in this figure legend, the reader is referred to the Web version of this article.)

loaded on adhesive hydrogels for implantation during RC repair. Compared with USC-Exos, CD133$^+$ USC-Exos could promote the healing of BTI more effectively from histological and biomechanical tests, which might be related to the stimulation of BMSCs to chondroblast differentiation. The results suggested that the CD133$^+$ USC-Exos hydrogel complex may become a promising stem cell exosome-based clinical treatment for RC healing.

In the past few decades, mesenchymal stem cells and their derived exosomes have shown great potential in tissue regeneration and repair. Huang Y et al. found that BMSC-Exos promote RC healing by promoting angiogenesis in rats and regulating M1 macrophages [10]. Wang C et al. found that ADSC-Exos reduced fatty infiltration and promoted regeneration of the fibrocartilage layer in a rabbit RC injury model to enhance RC healing [11]. Obtaining exosomes from mesenchymal stem cells, such as bone marrow and adipose tissue, usually has limited sources and involves invasive procedures. USCs and their exosomes have attracted much attention in regenerative medicine due to their simpler and non-invasive acquisition. Under certain induction conditions, USCs can differentiate into osteoblasts, chondrocytes, and adipocytes [31]. Recently, mesenchymal stem cells and their derived exosomes have shown great potential in RC regeneration and repair, and the acquisition of stem cell subpopulations based on the expression of specific surface molecules has received more attention [18]. Therefore, it is necessary to find a group of cells with stronger differentiation ability. Inspired by Chen AJ et al. [21], we successfully identified USCs with fixed expressions of CD29, CD44, CD73, and CD90, but negative expressions for CD34 and CD45. The USC subsets with an expression of CD133 were then sorted by flow cytometry. Our in vitro results confirmed that the isolated CD133$^+$ USCs showed stronger chondrogenic differentiation capacity. In this study, we found no significant difference between CD133$^+$ USCs and USCs in osteogenic ability, and the exosomes from the above cells showed consistent performance in promoting subchondral bone repair. But Chen AJ et al. found that spindle-shaped USCs has strong osteogenic ability [21]. The reason may be that we obtained a higher percentage of CD133 positive cells by flow sorting. The proportion of CD133$^+$ USCs may affect the overall osteogenic capacity of cells and reduce the statistical difference. We will conduct further research in the future. Aiming to better deliver the exosomes from urine-derived stem subpopulation to the injury site, we chose to mix hydrogel and the CD133$^+$ USC-Exos or USC-Exos to form a sustained-release system for local transplantation to reduce the degradation of exosomes. The results showed that Exo adhered well to the local insertion and continued to be released until 14 days after RC injury, which meant that the sustained benefits of CD133$^+$ USC-Exos or USC-Exos could last at least 14 days after RC injury.

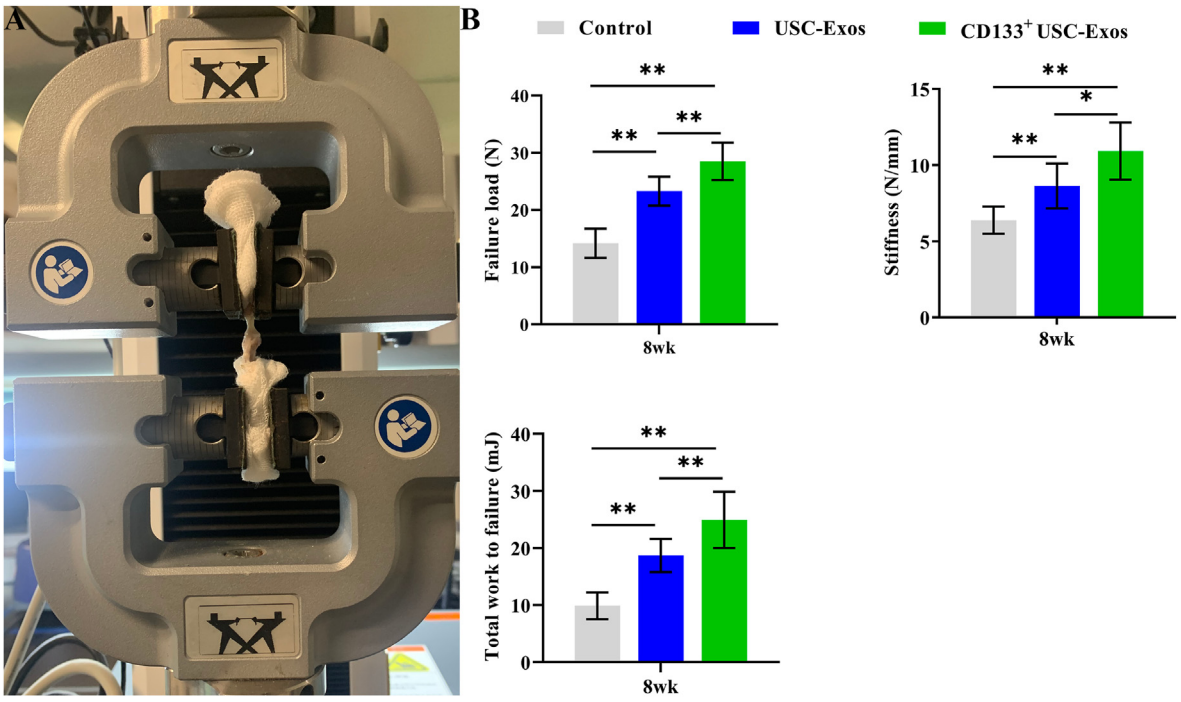

Fig. 8. Biomechanical testing of the supraspinatus tendon-humeral complex specimens at 8 weeks after surgery among the Control, USC-Exos, and CD133$^+$ USC-Exos. (A) Representative biomechanical testing images of clamping setup. (B) Quantitative analysis of failure load, stiffness, and total work to failure. n = 8 per group. Data are showed as means ± standard deviation (*$P < 0.05$, **$P < 0.01$).

Mesenchymal stem cells can migrate and chemotactic to damaged parts of the body, and can differentiate into tissue-specific cells to replace damaged or lost cells in the specific local microenvironment of damaged tissue [32]. Yet the decreased ability of mesenchymal stem cells to migrate or differentiate may lead to poor healing outcomes [33]. Some studies have found that tendon-derived cells may not be the main cells for BTI healing [34], but bone marrow-derived cells may be the main cells [35]. Kida Y et al. suggested that bone marrow-derived precursor cells enter the BTI through the bone tunnel to promote RC healing [36]. Jo CH et al. found that multiple channeling significantly decreased the retear rate after arthroscopic rotator cuff repair, probably via the recruitment of endogenous MSCs from the proximal humerus [37]. Therefore, we chose to investigate into BMSCs (Fig. S2), which may be closely related to BTI healing, as the object of experimental study in vitro.

Our in vitro experimental results showed that both CD133$^+$ USC-Exos and USC-Exos could be efficiently taken up by BMSCs and promoted their migration, osteogenic, and chondrogenic differentiation. However, exosomes from CD133$^+$ USCs induced better chondrogenic differentiation of BMSCs than USC-Exos. Consistent with the in vivo results, we found that CD133$^+$ USC-Exos can more effectively promote the regeneration of BTI fibrocartilage, which may be related to its ability to promote the differentiation of BMSCs into chondrogenesis. What's more, CD133$^+$ USC-Exos significantly promoted the SOX9 expression in BTI at 2 weeks postoperatively (Fig. S2). Taken together, we have reasons to speculate that the healing effect of CD133$^+$ USC-Exos on BTI regeneration may be mediated by the activation of BMSCs. Subsequent biomechanical testing found that the CD133$^+$ USC-Exos group had the best biomechanical properties compared to the control and USC-Exos groups. These changes in fibrocartilage formation may be partly responsible for the differences in biomechanical properties between the CD133$^+$ USC-Exos group and the remaining groups, as fibrocartilage formation has been reported to be closely related to the quality of insertion healing [38,39].

This study has certain limitations. Firstly, although this model has been widely used to study RC injury healing mechanisms and methods to enhance healing, there are still differences between rats and humans in terms of anatomy and healing ability. In addition, this is an acute injury model while RC injuries in humans may be chronic. The findings in this rat model may not be directly applicable to humans. Secondly, we only studied the effectiveness of exosomes in male subjects, and the experimental results may be biased by ignoring gender differences. Thirdly, although it was observed in our study that CD133$^+$ USC-Exos and USC-Exos can promote the migration, osteogenic and chondrogenic differentiation of BMSCs in vitro, there is no direct in vivo data showing the effects of the two on the functional properties of BMSCs. We also only found that CD133$^+$ USC-Exos and USC-Exos affect the biological behavior of BMSCs in vitro and did not study their effects on other stem cells. Fourthly, the total amount of exosome administration used in our in vivo experiments was 100 μg. Although this dose of CD133$^+$ USC-Exos and USC-Exos was effective for BTI healing, it will be meaningful to further optimize the dose to more effectively promote BTI healing. Lastly, future studies can be used to identify active components of CD133$^+$ USC-Exos that are more effective in promoting fibrocartilage regeneration than USC-Exos through miRNA analysis or proteomic analysis.

7. Conclusion

In the present study, we investigated for the first time the effects of USC-Exos and CD133$^+$ USC-Exos on RC healing in rats. The results showed that local injection of CD133$^+$ USC-Exos into the insertion site could improve the healing quality of BTI more effectively than USC-Exos hydrogel complex, which may be related to the activation of BMSCs by CD133$^+$ USC-Exos towards chondrogenic differentiation. We believe that the CD133$^+$ USC-Exos hydrogel complex may become a promising stem cell exosome-based clinical treatment for RC healing.

Author contributions

X.T., Y.X. acquisition of data, development of methodology, analysis of data, interpretation of data, drafting the manuscript. T.Z., J.X., and C.D.: assisted in the experiments and preparation of the manuscript. D.X.

and D.S: study design, project administration. D.X., T.Z.: paper revision, method advice. Xiaopeng Tong and Yan Xu contributed equally to this work. All authors read and approved the final manuscript.

Funding

This work was supported by the National Natural Science Foundation of China (No.81974338 and No.81730068), the Science and Technology Major Project of Changsha (No.kh2102015), and the Research and Development Program in Key Areas of Hunan Province (No.2020SK2077).

Declaration of competing interest

The authors declare that no conflicts of interest exist.

Acknowledgments

The authors would like to thank professor Hui Xie and other staff from Movement System Injury and Repair Research Center, Xiangya Hospital, Central South University, Changsha, China, for their kind assistance during the experiment.

Appendix A. Supplementary data

Supplementary data to this article can be found online at https://doi.org/10.1016/j.jot.2023.02.002.

References

[1] Oh LS, Wolf BR, Hall MP, Levy BA, Marx RG. Indications for rotator cuff repair: a systematic review. Clin Orthop Relat Res 2007;455:52–63.
[2] Hakimi O, Mouthuy PA, Carr A. Synthetic and degradable patches: an emerging solution for rotator cuff repair. Int J Exp Pathol 2013;94(4):287–92.
[3] Klouche S, Lefevre N, Herman S, Gerometta A, Bohu Y. Return to sport after rotator cuff tear repair: a systematic review and meta-analysis. Am J Sports Med 2016;44(7):1877–87.
[4] Sears BW, Choo A, Yu A, Greis A, Lazarus M. Clinical outcomes in patients undergoing revision rotator cuff repair with extracellular matrix augmentation. Orthopedics 2015;38(4):e292–6.
[5] Bjornsson HC, Norlin R, Johansson K, Adolfsson LE. The influence of age, delay of repair, and tendon involvement in acute rotator cuff tears: structural and clinical outcomes after repair of 42 shoulders. Acta Orthop 2011;82(2):187–92.
[6] Genin GM, Thomopoulos S. The tendon-to-bone attachment: unification through disarray. Nat Mater 2017;16(6):607–8.
[7] Valencia Mora M, Ruiz Iban MA, Diaz Heredia J, Barco Laakso R, Cuellar R, Garcia Arranz M. Stem cell therapy in the management of shoulder rotator cuff disorders. World J Stem Cell 2015;7(4):691–9.
[8] Kalluri R, LeBleu VS. The biology, function, and biomedical applications of exosomes. Science 2020;367(6478).
[9] He C, Zheng S, Luo Y, Wang B. Exosome theranostics: biology and translational medicine. Theranostics 2018;8(1):237–55.
[10] Huang Y, He B, Wang L, Yuan B, Shu H, Zhang F, et al. Bone marrow mesenchymal stem cell-derived exosomes promote rotator cuff tendon-bone healing by promoting angiogenesis and regulating M1 macrophages in rats. Stem Cell Res Ther 2020;11(1):496.
[11] Wang C, Hu Q, Song W, Yu W, He Y. Adipose stem cell-derived exosomes decrease fatty infiltration and enhance rotator cuff healing in a rabbit model of chronic tears. Am J Sports Med 2020;48(6):1456–64.
[12] Zhang Y, McNeill E, Tian H, Soker S, Andersson KE, Yoo JJ, et al. Urine derived cells are a potential source for urological tissue reconstruction. J Urol 2008;180(5):2226–33.
[13] Ji X, Wang M, Chen F, Zhou J. Urine-derived stem cells: the present and the future. Stem Cell Int 2017;2017:4378947.
[14] Bharadwaj S, Liu G, Shi Y, Wu R, Yang B, He T, et al. Multipotential differentiation of human urine-derived stem cells: potential for therapeutic applications in urology. Stem Cell 2013;31(9):1840–56.
[15] Wu S, Liu Y, Bharadwaj S, Atala A, Zhang Y. Human urine-derived stem cells seeded in a modified 3D porous small intestinal submucosa scaffold for urethral tissue engineering. Biomaterials 2011;32(5):1317–26.
[16] Guan J, Zhang J, Zhu Z, Niu X, Guo S, Wang Y, et al. Bone morphogenetic protein 2 gene transduction enhances the osteogenic potential of human urine-derived stem cells. Stem Cell Res Ther 2015;6:5.
[17] Chen L, Li L, Xing F, Peng J, Peng K, Wang Y, et al. Human urine-derived stem cells: potential for cell-based therapy of cartilage defects. Stem Cell Int 2018;2018:4686259.
[18] Mo M, Wang S, Zhou Y, Li H, Wu Y. Mesenchymal stem cell subpopulations: phenotype, property and therapeutic potential. Cell Mol Life Sci 2016;73(17):3311–21.
[19] Goncalves AI, Gershovich PM, Rodrigues MT, Reis RL, Gomes ME. Human adipose tissue-derived tenomodulin positive subpopulation of stem cells: a promising source of tendon progenitor cells. J Tissue Eng Regen Med 2018;12(3):762–74.
[20] Yin Z, Hu JJ, Yang L, Zheng ZF, An CR, Wu BB, et al. Single-cell analysis reveals a nestin(+) tendon stem/progenitor cell population with strong tenogenic potentiality. Sci Adv 2016;2(11):e1600874.
[21] Chen AJ, Pi JK, Hu JG, Huang YZ, Gao HW, Li SF, et al. Identification and characterization of two morphologically distinct stem cell subpopulations from human urine samples. Sci China Life Sci 2020;63(5):712–23.
[22] Cao Y, Xu Y, Chen C, Xie H, Lu H, Hu J. Local delivery of USC-derived exosomes harboring ANGPTL3 enhances spinal cord functional recovery after injury by promoting angiogenesis. Stem Cell Res Ther 2021;12(1):20.
[23] Xu Y, Zhang T, Chen Y, Shi Q, Li M, Qin T, et al. Isolation and characterization of multipotent canine urine-derived stem cells. Stem Cell Int 2020;2020:8894449.
[24] Luo Z, Peng W, Xu Y, Xie Y, Liu Y, Lu H, et al. Exosomal OTULIN from M2 macrophages promotes the recovery of spinal cord injuries via stimulating Wnt/beta-catenin pathway-mediated vascular regeneration. Acta Biomater 2021;136:519–32.
[25] Kilkenny C, Browne WJ, Cuthill IC, Emerson M, Altman DG. Improving bioscience research reporting: the ARRIVE guidelines for reporting animal research. PLoS Biol 2010;8(6):e1000412.
[26] Plate JF, Brown PJ, Walters J, Clark JA, Smith TL, Freehill MT, et al. Advanced age diminishes tendon-to-bone healing in a rat model of rotator cuff repair. Am J Sports Med 2014;42(4):859–68.
[27] Ide J, Kikukawa K, Hirose J, Iyama K, Sakamoto H, Fujimoto T, et al. The effect of a local application of fibroblast growth factor-2 on tendon-to-bone remodeling in rats with acute injury and repair of the supraspinatus tendon. J Shoulder Elbow Surg 2009;18(3):391–8.
[28] Chen C, Chen Y, Li M, Xiao H, Shi Q, Zhang T, et al. Functional decellularized fibrocartilaginous matrix graft for rotator cuff enthesis regeneration: a novel technique to avoid in-vitro loading of cells. Biomaterials 2020;250:119996.
[29] Tao SC, Guo SC, Zhang CQ. Modularized extracellular vesicles: the dawn of prospective personalized and precision medicine. Adv Sci (Weinh) 2018;5(2):1700449.
[30] Tkach M, Thery C. Communication by extracellular vesicles: where we are and where we need to go. Cell 2016;164(6):1226–32.
[31] Guan JJ, Niu X, Gong FX, Hu B, Guo SC, Lou YL, et al. Biological characteristics of human-urine-derived stem cells: potential for cell-based therapy in neurology. Tissue Eng 2014;20(13–14):1794–806.
[32] Uccelli A, Moretta L, Pistoia V. Mesenchymal stem cells in health and disease. Nat Rev Immunol 2008;8(9):726–36.
[33] Fu X, Liu G, Halim A, Ju Y, Luo Q, Song AG. Mesenchymal stem cell migration and tissue repair. Cells 2019;8(8).
[34] Kinneberg KR, Galloway MT, Butler DL, Shearn JT. The native cell population does not contribute to central-third graft healing at 6, 12, or 26 weeks in the rabbit patellar tendon. J Orthop Res 2013;31(4):638–44.
[35] Rothrauff BB, Tuan RS. Cellular therapy in bone-tendon interface regeneration. Organogenesis 2014;10(1):13–28.
[36] Kida Y, Morihara T, Matsuda K, Kajikawa Y, Tachiiri H, Iwata Y, et al. Bone marrow-derived cells from the footprint infiltrate into the repaired rotator cuff. J Shoulder Elbow Surg 2013;22(2):197–205.
[37] Jo CH, Shin JS, Park IW, Kim H, Lee SY. Multiple channeling improves the structural integrity of rotator cuff repair. Am J Sports Med 2013;41(11):2650–7.
[38] Lu H, Qin L, Cheung W, Lee K, Wong W, Leung K. Low-intensity pulsed ultrasound accelerated bone-tendon junction healing through regulation of vascular endothelial growth factor expression and cartilage formation. Ultrasound Med Biol 2008;34(8):1248–60.
[39] Chen Y, Zhang T, Wan L, Wang Z, Li S, Hu J, et al. Early treadmill running delays rotator cuff healing via Neuropeptide Y mediated inactivation of the Wnt/beta-catenin signaling. J Orthop Translat 2021;30:103–11.